Tertiary Control of Voltage Unbalance Compensation for Optimal Power Quality in Islanded Microgrids

Meng, Lexuan; Tang, Fen; Savaghebi, Mehdi; Quintero, Juan Carlos Vasquez; Guerrero, Josep M.

Published in:
I E E E Transactions on Energy Conversion

DOI (link to publication from Publisher):
10.1109/TEC.2014.2363687

Publication date:
2014

Document Version
Early version, also known as pre-print

Tertiary Control of Voltage Unbalance Compensation for Optimal Power Quality in Islanded Microgrids

Lexuan Meng, Fen Tang, Mehdi Savaghebi, Juan C. Vasquez, Josep M. Guerrero

***Abstract*—In multi-bus islanded microgrids, the power quality requirements for different areas and buses can be different. This paper proposes a hierarchical control to realize optimal unbalance compensation for satisfying the power quality requirements in different areas. Primary and secondary controllers are applied to realize unbalance compensation for critical bus (CB) and at the same time, to make distributed generators (DGs) equally share the compensation efforts. Tertiary control, which inherently is an optimization method, is implemented to adjust the compensating effort of each DG considering the voltage unbalance limits in local buses and DG terminals. This method realizes multi-power-quality-level control in a multi-bus islanded system by optimally utilizing DGs as distributed compensators and saves the investment for additional compensation equipment. Hardware-in-the-loop results demonstrate the effectiveness of the method.**

***Index Terms*--microgrid, tertiary control, voltage unbalance compensation, multi-power-quality-level**

NOMENCLATURE

A	Transformation matrix between 3-phase system and symmetrical sequence system.
CB	Critical bus.
DG	Distributed generation.
E_0	Rated voltage amplitude.
E^*	Reference of voltage amplitude.
f_c	Cut-off frequency of the low pass filter.
f_{obj}	Objective function.
f_{syn}	Synthesized objective function.
ϕ^*	Reference of phase angle.
GA	Genetic algorithm.
G_V, G_I	Transfer functions of voltage and current loops.
g_{LB},g_{DG},g_{PHC}	Constraining functions for *VUF* on LBs, *VUF* on DG sides and DGs' phase current value.
HIL	Hardware-in-the-loop.
h_{bi}	A variable with value 0 or 1 denoting if the i^{th} bus is taken into optimization.
$\dot{I}^{P/N/Z}$	Positive-/negative-/zero sequence current phasor.
$I_{Si}^{P/N}$	Positive-/negative sequence output current of i^{th} DG unit.
I_{ss}	Current in symmetrical sequence system.
I_{oa}, I_{ob}, I_{oc}	Output phase current of i^{th} DG.
$I_{PHi}^{\max}$	Upper limit of the phase current peak value of i^{th} DG unit.
$i_{o\alpha\beta}^{+}$	Positive sequence currents in $\alpha\beta$ reference.
$k_{f/GLB/GDG/GC}$	Coefficients defining the influence of objective function and constraints.
k_{LBi}	A variable denoting the relative importance of the i^{th} LB.
k_{pV}, k_{rV}	Proportional and resonant coefficients of the inner voltage loop.
k_{pI}, k_{rI}	Proportional and resonant coefficients of the inner current loop.
LBCL	Low bandwidth communication link.
LC	Local controller.
LPF	Low pass filter.
L_V	Virtual inductance.
MGCC	Microgrid central controller.
MPQL	Multiple-power-quality-level.
m	Total number of buses.
m_P, m_D	Proportional and derivative coefficients of active power droop controller.
n	Total number of compensating DGs.
n_P	Proportional coefficient of reactive power droop controller.
PI	Proportional integral.
P^+, Q^+	Positive sequence active and reactive power.
par_i	Population generated by GA ($par_i \in (0,1)$).
R_{TCG}	Ratio between *TCG* values.
R_V	Virtual resistance.

Lexuan Meng, Mehdi Savaghebi, Juan C. Vasquez, Josep M. Guerrero are with Department of Energy Technology, Aalborg University, 9220 Aalborg (e-mail: lme@et.aau.dk; mhsavagh@gmail.com; juq@et.aau.dk; joz@et.aau.dk).

Fen Tang is with School of Electrical Engineering, Beijing Jiaotong University (e-mail: ftang_nego@126.com).

r_{LBi}, r_{DGi}, r_{Ci}	Penalty factors for the *VUF* violation on the i^{th} LB, the *VUF* violation on the i^{th} DG, and the violation of phase current constraint of i^{th} DG.
SLB	Sensitive load bus.
s	Laplace operator.
TCG	Tertiary compensation gain.
UCR	Unbalance compensation reference.
VUF	Voltage unbalance factor.
$\dot{V}^{P/N}$	Positive-/negative sequence voltage phasor.
$V_{LBi}^{P/N}$, $V_{CBi}^{P/N}$	Positive-/negative sequence voltage at local bus and critical bus.
V_{ph}	Phase voltage in 3-phase system.
$V_{S\_total}^{N}$	Sum of the negative sequence voltages in all the DG sides.
$V_{Si}^{P/N}$	Positive-/negative sequence output voltage of i^{th} DG.
V_{ss}	Voltage and current in symmetrical sequence system.
$VUF_{LBi/CB}$	*VUF* on LB/CB.
$VUF_{LBi/DGi}^{\max}$	Upper limits of *VUF* value on LB or DG sides.
$v_{V\alpha}$, $v_{V\beta}$	Voltage reference generated by virtual impedance loop.
ω	Angular frequency.
ω^{*}	Reference of angular frequency.
ω_0	Rated angular frequency.
ω_{cV}, ω_{cI}	Cut-off angular frequencies of the inner voltage and current controllers.
Y, Y_u	Admittances of loads.
$Y_{oi}^{P/N}$, $Y_i^{P/N}$	Positive-/negative sequence admittances of distribution lines.
Y_{ph}	Admittance matrix in 3-phase system.
Y_{ss}	Admittance matrix in symmetrical sequence system.

I. Introduction

THE ongoing revolution in electric power system is marked by the increasing penetration of renewable energy sources, distributed generation (DG) and energy storage systems aiming at efficient operation of the whole electric power system. As a way of actualizing this new paradigm, microgrid concept [1][2] has been proposed for liberalizing the operation of each system fraction and providing consumer with reliable power supply and desirable power quality. However, voltage unbalances usually exist in three-phase system when the transmission lines are unsymmetrical or single-phase loads are connected, which may cause more power losses and affect the system stability. The performance of equipment which is sensitive to voltage unbalance such as induction motors can be deteriorated. Conventionally, series active power filter can be

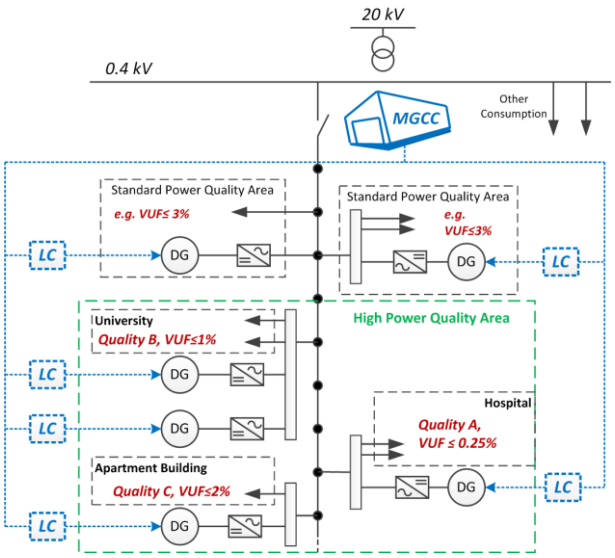

Fig. 1. Centralized control in a low voltage microgrid.

a solution for compensating unbalances by adding negative sequence voltage in series with the distribution line [3]-[5]. In some works shunt active filters are used to inject negative sequence current to balance the current in the distribution lines and consequently compensate unbalances [6]-[8]. However, all these methods require additional compensation equipment which may increase the total investment cost.

In case of microgrids, in order to make full use of DG units, the compensation function can be integrated into DG local controllers in order to employ DG units as active filters and compensators [9]-[11]. This concept is enabled by prevalent utilization of interfacing inverters and the advanced sensing, monitoring and communication techniques. In addition, the compensation efforts can be shared among DGs [12]-[16].

A hierarchical control is proposed in [15] and [16] to compensate voltage unbalance in sensitive load bus (SLB) of an islanded microgrid. The hierarchy consists of two levels: primary (local) and secondary (central). A compensating reference is generated by secondary controller and sent to primary controller. Then every primary controller follows the compensating reference and controls the DG to compensate unbalances in the point of common coupling. This method is able to equalize the compensation efforts shared among DG units despite of distribution line differences and load changes.

However, in order to ensure the highest power quality in SLB the above mentioned method is actually sacrificing the power quality in DG terminals and other buses without considering their local power quality limitations and the power rating of each DG unit. The power quality requirements are usually distinguished in different areas depending on the type of electric appliances [17]. It can be more convenient to differentiate the power quality levels for different types of electric consumers. A project in the Consortium for Electric Reliability Technology Solutions (CERTS) [18] and a four-year project in Sendai, Japan, [19]-[21] have demonstrated the need for multiple-power-quality-level (MPQL) service for future grids. A power quality control center is established to differentiate the power quality level for different areas.

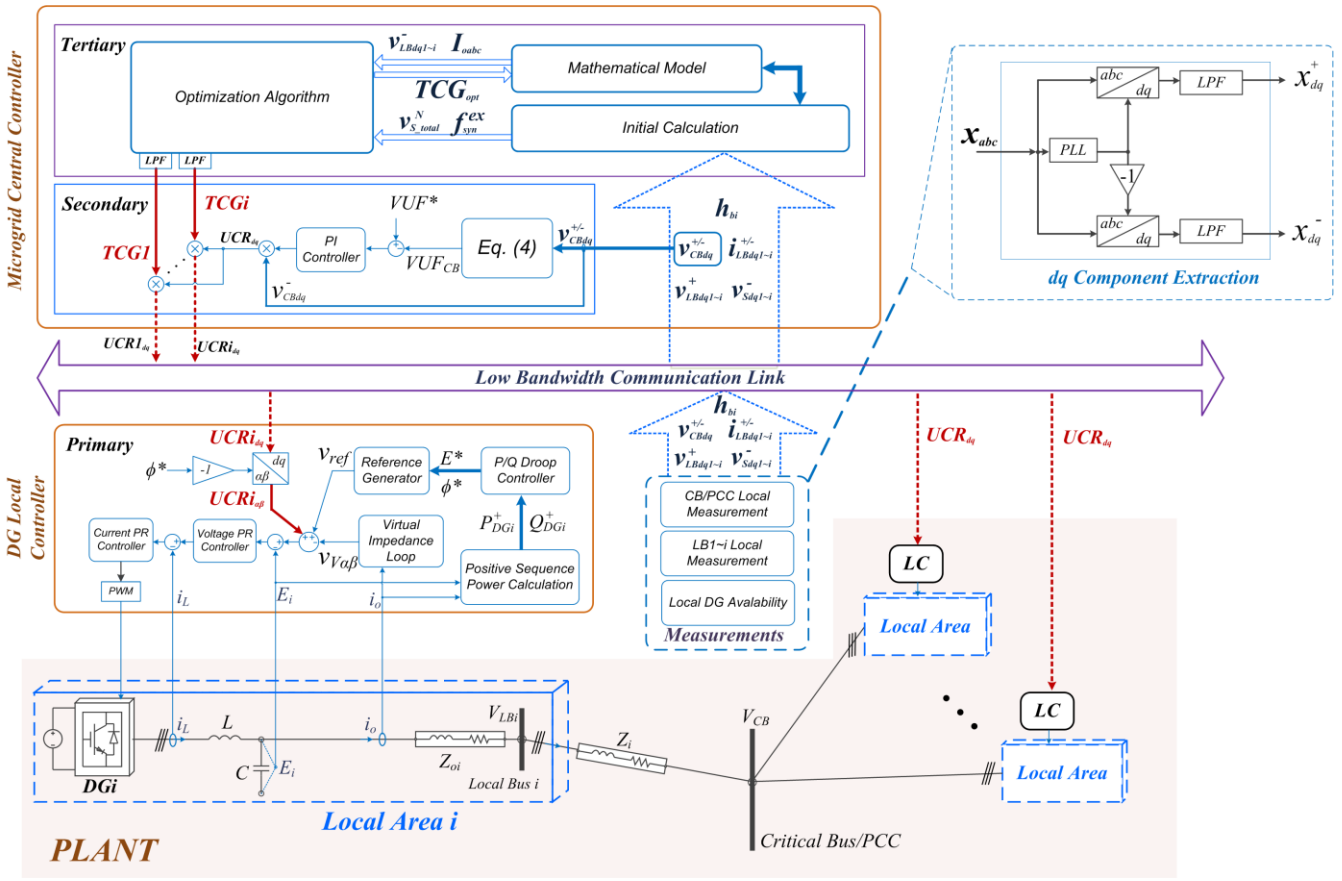

Fig. 2. Hierarchical control scheme for unbalance compensation and MPQL control.

Instead of using extra compensation equipment, which may bring more cost, this paper proposes a tertiary control to employ DGs as distributed compensators, and achieve optimal unbalance compensation and MPQL control. A small-scale low voltage benchmark microgrid [22] is considered in this paper as shown in Fig. 1. Assume that high power quality area (*Quality A*) only accepts low level of voltage unbalance while the *Quality B* and *C* areas can accept more unbalances but have certain limits. A hierarchical control including primary, secondary and tertiary control levels is proposed to achieve this goal. The primary level is usually implemented in local controller (LC), while the secondary and tertiary controllers are integrated in the microgrid central controller (MGCC).

The paper is organized as follows. Section II introduces the proposed hierarchical control for optimal unbalance compensation and MPQL control. Section III analyzes and models the unbalanced system. A small-scale microgrid (2-DG, 3-bus) is also described and taken as the example system of this study. Based on this model, Section IV formulates the general mathematical model for voltage unbalance compensation optimization. Hardware-in-the-loop results in Section V demonstrate the effectiveness of the method. Section VI provides the conclusions.

II. Hierarchical Control for Voltage Unbalance Compensation and MPQL Control

Hierarchical control is usually applied for the proper control of microgrids to achieve control objectives in different time scales, regional areas and physical levels. The hierarchy is organized in three levels [23]:

1) *Primary level*: primary control performs the function of power sharing among DG units. Droop method is often applied in this level.
2) *Secondary level*: secondary control focuses on the restoration of frequency and voltage deviation caused by droop control as well as power quality issues.
3) *Tertiary level*: tertiary control deals with economic related issues, such as optimal dispatching, operation scheduling and optimization for different objectives.

Based on this definition, this paper proposes a hierarchical control for actualizing optimal unbalance compensation and MPQL control, as shown in Fig. 2.

An example islanded microgrid is outlined in the *PLANT* block depicted in Fig. 2. The DG power stage is represented by a power electronics inverter, which is usually used for controlling the active and reactive power injection. One or more DG units are connected to a local bus (LB) to supply local loads. A critical bus (CB), which contains critical loads and power-quality sensitive loads, may exist in the system. In order to keep the safe operation of the system and to protect critical loads in CB, DG units should ensure that CB has the highest power quality. However, voltage unbalances may appear when unbalanced loads are connected, causing voltage unbalance in different buses and affecting the system stability and security. In order to achieve better power quality in the CB, DG units can be employed as distributed active

compensators to share the compensation efforts by means of secondary and primary controllers. Furthermore, considering the distribution line differences, DG compensation capabilities, as well as different power quality requirements in DG side and other buses, a tertiary control may be needed to redistribute the sharing of compensation efforts among DG units to achieve optimum operation objectives.

A. Primary Control and Inner Control Loops

The control structure of local controller is shown in the *Primary* block in Fig. 2, which includes current and voltage control loops, active and reactive power droop control loops and virtual impedance loops. All the control loops are designed in $\alpha\beta$ frame. The output active and reactive power of the inverter is first calculated based on the instantaneous power theory [24]. Positive sequence active and reactive power (P^+ and Q^+) can be extracted by using *low pass filters* (LPF) [15], [16]. The calculated P^+ and Q^+ are then used by droop controller for P^+/Q^+ sharing control, as defined in [15]:

$$\begin{cases} \phi^* = \dfrac{\omega^*}{s} = \dfrac{1}{s}\left[\omega_0 - \left(m_P + m_D \cdot s\right)P^+\right] \\ E^* = E_0 - n_P \cdot Q^+ \end{cases} \tag{1}$$

In addition to droop control, a virtual impedance loop is implemented [15]:

$$\begin{cases} v_{V\alpha} = R_V \cdot i_{o\alpha}^+ - \omega L_V \cdot i_{o\beta}^+ \\ v_{V\beta} = R_V \cdot i_{o\beta}^+ + \omega L_V \cdot i_{o\alpha}^+ \end{cases} \tag{2}$$

In order to track non-dc variables, proportional-resonant controllers are used to control voltage and current [15]:

$$\begin{cases} G_V(s) = k_{pV} + \dfrac{2k_{rV} \cdot \omega_{cV} \cdot s}{s^2 + 2\omega_{cV} \cdot s + \omega_0^2} \\ G_I(s) = k_{pI} + \dfrac{2k_{rI} \cdot \omega_{cI} \cdot s}{s^2 + 2\omega_{cI} \cdot s + \omega_0^2} \end{cases} \tag{3}$$

B. Secondary Control Loop

Secondary control loops deal with CB voltage unbalance compensation by sending Unbalance Compensation Reference (UCR_{dq}) to local controllers through *low bandwidth communication links* (LBCL). As shown in Fig. 2, the positive and negative sequence voltages of CB ($v_{CBdq}^{+/-}$) are measured locally and sent to MG central controller. The *measurements* and *dq component extraction* blocks are given in Fig. 2. LPFs with cut-off frequency f_{cut}=2Hz are applied to extract critical components. Voltage unbalance factor (*VUF*) at CB can be calculated as follows [25]:

$$VUF_{CB} = 100 \cdot \sqrt{\frac{(v_{CBd}^-)^2 + (v_{CBq}^-)^2}{(v_{CBd}^+)^2 + (v_{CBq}^+)^2}} \tag{4}$$

It is noteworthy that the calculation delay has to be considered when applying the secondary and tertiary functions. The delay is mainly caused by the using of LPFs. In this paper, the f_{cut} is set to 2Hz, and the secondary and tertiary control parameters are tuned and tested under this value. Then the error between calculated *VUF* and reference VUF^* is fed to a proportional-integral (*PI*) controller. The output of *PI* controller is multiplied by v_{CBdq}^- to generate the common compensation reference UCR_{dq} [15]:

$$UCR_{dq} = v_{CBdq}^- \cdot \left[\left(\frac{k_i}{s} + k_p\right) \cdot (VUF^* - VUF_{CB}) \right] \tag{5}$$

In each local primary controller, the UCR_{dq} is transformed to $\alpha\beta$ frame where $-\phi^*$ is used as the rotation angle as the transformation is executed over negative sequence values.

C. Tertiary Control Loop

With secondary control the voltage unbalance on CB can be compensated by DGs. However, considering the compensation limitations of DGs and power quality requirements in different LBs, the compensation efforts need to be optimally distributed. In this paper, it is actualized by multiplying a tertiary compensation gain (*TCG*) to the compensation reference UCR_{dq} before it is sent to local controllers. In addition, LPFs are needed between tertiary control and secondary control so as to smooth the change of the *TCG* values. The cut-off frequency of the LPFs is set to 2Hz.

With centralized control system, essential information can be collected by using LBCLs to execute optimization function. The optimization objective in this paper is to control *VUF* on different LBs to desirable levels by changing *TCG*s. However, there is no straight-forward relationship between *TCG* and LB *VUF* values. The challenges are the modeling and analysis of the unbalance system as well as the formulation of the mathematical problem. Accordingly, the modelling and analysis of the unbalance system are presented in Section III. The detailed optimization problem formulation and tertiary control algorithm are stated in Section IV.

III. Unbalance System Modeling

As radial networks are often used in microgrids, a 2-DG 3-Bus islanded system is taken as an example with the single-line diagram shown in Fig. 3 (a). Assuming that the transmission line admittances can be estimated as Y_{o1}, Y_1 and Y_{o2}, Y_2, the objective is to obtain a negative sequence equivalent circuit, as shown in Fig. 3 (b), for analyzing negative sequence voltage changes in each bus.

However, the negative sequence quantities cannot be considered separately from positive sequence. Assuming the presence of unbalanced loads in different buses, as that shown in Fig. 4, the sequence quantities of the system can be calculated based on classical methods [26]:

$$\begin{cases} Y_{ss} = A^{-1} \cdot Y_{ph} \cdot A \\ V_{ss} = A^{-1} \cdot V_{ph} \\ I_{ss} = Y_{ss} \cdot V_{ss} \end{cases} \tag{6}$$

Detailed matrices are given in the *Appendix*. The positive and negative sequence currents can be obtained by solving (6) (a used in the following equation is equal to $1\angle 120°$):

$$\begin{cases} \dot{I}^P = \dot{V}^P \cdot Y + (\dot{V}^P - a \cdot \dot{V}^N) \cdot Y_u \\ \dot{I}^N = \dot{V}^N \cdot Y + (\dot{V}^N - a^2 \cdot \dot{V}^P) \cdot Y_u \end{cases} \tag{7}$$

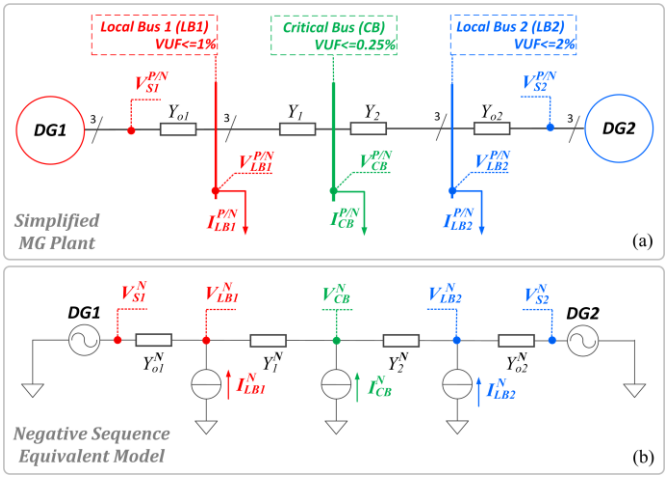

Fig. 3. Example system and its negative sequence equivalent circuit: (a) example of islanded microgrid; (b) negative sequence equivalent model.

In addition, considering the facts that the maximum allowed voltage unbalance in power systems is 3% as defined by *ANSI C84.1-1995* [17], the positive sequence voltage is much larger than negative sequence voltage. When *VUF* value is within the range 0-5%, the value of the neglected term $\dot{V}^N \cdot Y + \dot{V}^N \cdot Y_u$ is always less than 5% of the nominal positive sequence current, which can be neglected even if under the condition that Y is much larger than Y_u. Accordingly, (7) can be well approximated as:

$$\begin{cases} \dot{I}^P \approx \dot{V}^P \cdot Y + \dot{V}^P \cdot Y_u \\ \dot{I}^N \approx -a^2 \cdot \dot{V}^P \cdot Y_u \end{cases} \tag{8}$$

It can be seen from (8) that the negative sequence current is determined by positive sequence voltage $\dot{V}^P$ and unbalanced load Y_u. In addition, as the voltage variation is bounded within 5% according to *IEEE Std 1547-2003* [27], the unbalanced load can be seen as a current source whose value is mainly determined by unbalanced load Y_u, as shown in Fig. 3 (b).

Based on the equivalent model and assuming that positive- and negative-sequence voltage and current can be measured locally and sent to central controller in *dq* reference frame for tertiary optimization, the negative-sequence electrical relationship among buses can be established based on Fig. 3 (b) as follows:

$$\dot{V}^N_{LB1} = (\dot{V}^N_{S1} \cdot Y^N_{o1} + \dot{V}^N_{CB} \cdot Y^N_1 + \dot{I}^N_{LB1}) / (Y^N_1 + Y^N_{o1}) \tag{9}$$

$$\dot{V}^N_{LB2} = (\dot{V}^N_{S2} \cdot Y^N_{o2} + \dot{V}^N_{CB} \cdot Y^N_2 + \dot{I}^N_{LB2}) / (Y^N_2 + Y^N_{o2}) \tag{10}$$

$$\dot{V}^N_{CB} = \frac{\dot{I}^N_{CB} + K_1 \cdot \dot{I}^N_{LB1} + K_2 \cdot \dot{I}^N_{LB2} + K_3 \cdot \dot{V}^N_{S1} + K_4 \cdot \dot{V}^N_{S2}}{K_3 + K_4} \tag{11}$$

where K_1, K_2, K_3, K_4 are constants (see *Appendix*).

A simplified compensation process can be sketched from (9)-(11), as shown in Fig. 5. The V_S^N axis represents the negative sequence voltage at both DG sides ($V^N_{S1} = V^N_{S2} = V^N_S$) while the V_B^N axis denotes the negative sequence voltage at buses. Assuming a case that $\dot{I}^N_{LB1} = \dot{I}^N_{LB2} = 0$ and $Y_1 < Y_2 < Y_{o1} = Y_{o2}$, it can be observed that without compensation ($V^N_S = 0$), the negative sequence voltage on CB and LBs is high, and the negative sequence voltage on LB2 is higher than that at LB1 due to the impedances difference of distribution lines. The

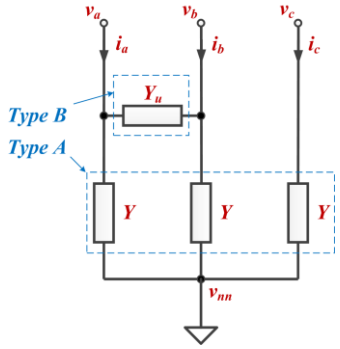

Fig. 4. Unbalanced load equivalent circuit in 3-phase 3-wire system.

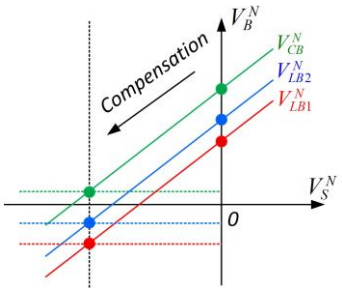

Fig. 5. Simplified compensation process.

secondary compensation control is actually adjusting the negative sequence voltage at DG side to reduce the negative sequence voltage in CB and LBs. After compensation, the negative sequence voltage at CB is kept at a low level, while the negative sequence voltage at LB1 and LB2 depends on the line impedance and local negative sequence current.

With secondary compensation, the power quality at CB can be kept at a low level (e.g. 0.25%), however, the *VUF* at LB1 and LB2 may be out of limits. Based on (9)-(11), an analysis can be conducted aiming at finding a desirable operation of the system to ensure proper voltage unbalance level in all buses.

An example case is set where $\dot{V}^N_{S1}$ and $\dot{V}^N_{S2}$ are changing in -10-10V range and distribution line admittances are set to $Y^N_{o1} = Y^N_{o2} = 2S$, $Y^N_1 = 1.25S$, $Y^N_2 = 2S$ (for the sake of simplicity, resistive network is considered here). Negative sequence load currents are set to $\dot{I}^N_{LB1} = 1A$, $\dot{I}^N_{LB2} = 5A$, $\dot{I}^N_{CB} = 10A$. The *VUF* limits in CB, LB1 and LB2 are set to 0.25%, 1% and 2%, respectively (see Fig. 3 (a)). The 3-dimensional figures in Fig. 6 indicate the *VUF* varying trends with the negative sequence voltage change in DG sides. The darkness denotes the level of *VUF*. Since the objective is to keep the *VUF* in each bus within acceptable limits, desirable area can be found in each figure. In Fig. 6 (a), the area between yellow dashed lines is the area where *VUF* is less than 1%. Actually, it is a constraint for the negative sequence voltage at DG1 side (V^N_{S1}). Similarly, an acceptable area (*VUF<=2%*) can be found in Fig. 6 (b) which actually constrains the negative sequence voltage at DG2 side (V^N_{S2}). In Fig. 6 (c), *VUF* at CB is plotted while considering the constraints obtained from Fig. 6 (a) and (b). The shadowed area is the desirable operation region for all the buses (LB1, LB2 and CB). However, if the two DGs equally share the compensation efforts, the operation point is located at the area marked by the blue circle on the diagonal dashed line. It can

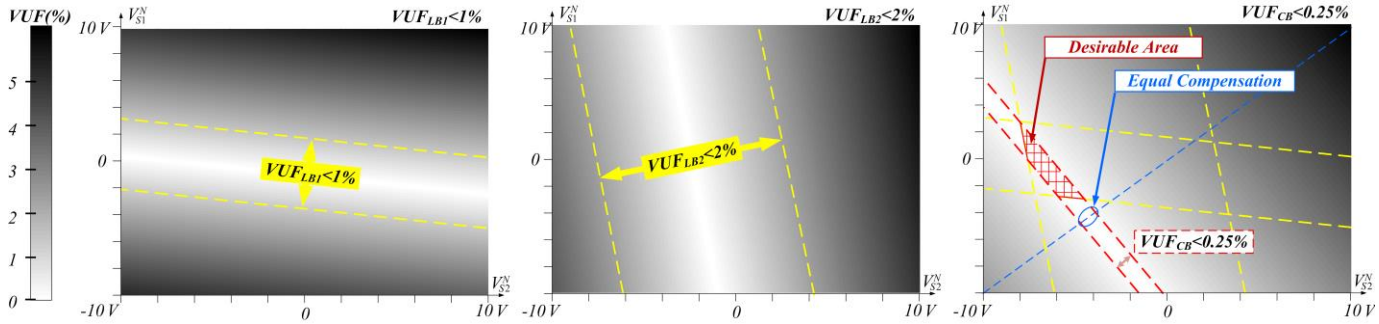

Fig. 6. *VUF* analysis regarding negative sequence voltage change on both DG sides.

be seen that it may be out of the desirable area. However, in order to make the system operate in the desirable area, the compensation efforts may not always be equally shared by DG units. An optimal ratio can be found to ensure proper operation. In addition, the optimal ratio changes with different unbalance levels and distribution line parameters.

Based on the above analysis, the objective of this paper is to keep the unbalance level on CB at a fixed low level, while controlling the unbalance level of LB1 and LB2 according to their power quality requirements and relative importance.

IV. Optimization Problem Formulation and Tertiary Control Implementation

In order to achieve the optimal unbalance compensation, the optimization problem is first formulated in this section. Genetic algorithm (GA) is used in this paper, as GA is a suitable algorithm for the kind of optimization problems related to analysis with complex models, such as the case presented in this paper. It offers many advantages, some of them are [28][29]: 1) it does not require derivative information of the objective function, so it can be applied to solve non-continuous, non-differentiable optimization problems; 2) it reduces the risk to be trapped in local optimal; 3) it can deal with a large number of variables while provide a list of solutions.

A. Optimization Problem Formulation

Based on the analysis and the model built in Section III, the optimization problem can be formulated. As CB is the most sensitive bus in the system, secondary control is in charge of keeping the best power quality on CB. *TCG*s can be used as decision variables to change the *VUF* on different LBs.

Accordingly, the objective of the tertiary control is to control the *VUF* on LBs to a desirable level according to the relative importance and *VUF* limit of the LB. The objective function can be formulated as [30]:

$$\min f_{obj} = \sum_{i=2}^{m} h_{bi}\left(k_{LB1}\cdot VUF_{LB1} - k_{LBi}\cdot VUF_{LBi}\right)^2 \qquad (12)$$

In addition, if the local DGs are not available to provide compensation support or they reach the P/Q generation limits [31]-[34], these DGs will not participate the compensation. In this case, the respective h_{bi} will be set to 0.

*TCG*s are used as decision variables to change the compensating effort of each DG. A mathematical relationship between *TCG* and *VUF* in LBs and DG sides is required. Furthermore, the sum of the *TCG*s has to be equal to the total number of compensating DGs so as to maintain the overall compensating efforts. Instead of adding constraint to *TCG* value, a simple and efficient method is used. In GA, the first population is generated within the range **(0,1)**. Then the *TCG* is calculated with regard to the total number of DG units:

$$\text{decision variables:}[TCG_1,...,TCG_i,...,TCG_n]$$

$$TCG_i = \frac{par_i}{\sum_{j=1}^{n} par_j}\cdot n \qquad (13)$$

GA helps to find the optimal sharing of compensation effort among DGs by manipulating the population, while (13) helps to keep the sum of *TCG* values equal to *n*. The mathematical relationship between *TCG*s and the electrical system can be established by:

$$V_{Si}^{N} = \frac{TCG_i}{\sum_{j=1}^{n} TCG_j}\cdot V_{S\_total}^{N} \qquad (14)$$

where $V_{S\_total}^{N}$ can be obtained by collecting and summing up the negative sequence voltages in all the DG sides. The total compensation efforts are regulated by secondary control to ensure required power quality in CB which conventionally is equally distributed to each DG unit [15], while (14) is actually a simple but effective approach that maintains the total amount of compensation efforts and adjusts the compensation effort of respective DG. The optimization is aimed at optimal distribution of $V_{S\_total}^{N}$. Equations (9), (10), (13) and (14) can be used by GA to evaluate the objective function with different populations.

Apart from objective function and decision variable, a set of constraints has to be taken into consideration:

1) Constraints applied to *VUF* on each LB (VUF_{LBi}, $i=1,2,\ldots,n$) and *VUF* on DG side (VUF_{DGi}, $i=1,2,\ldots,n$):

$$\begin{cases} 0 \le VUF_{LBi} \le VUF_{LBi}^{\max} \\ 0 \le VUF_{DGi} \le VUF_{DGi}^{\max} \end{cases} \qquad (15)$$

2) Constraints applied to current per phase value of each DG unit ($\{I_{oa}, I_{ob}, I_{oc}\}_{DGi}$, $i=1,2,\ldots,n$):

$$0 \le \{I_{oa}, I_{ob}, I_{oc}\}_{DGi} \le I_{PHi}^{\max} \qquad (16)$$

It is noteworthy that the active and reactive power of DGs are also limited according to standards and DG capability [31]-

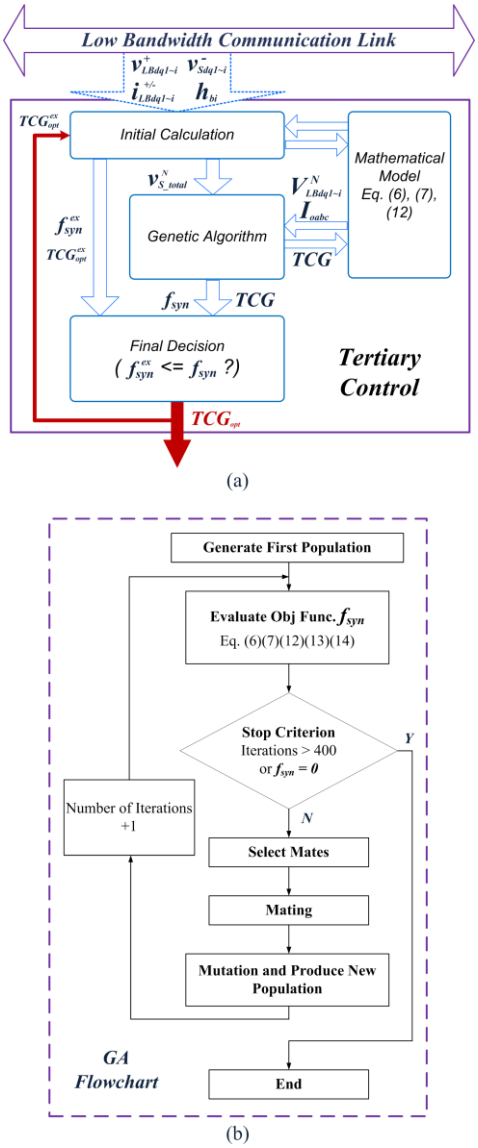

Fig. 7. Tertiary control: (a) structure of tertiary control and (b) GA flowchart.

[34]. These constraints can be considered as the availability of the local DGs to participate the compensation. If all the DGs in the local area reach generation limits, they will not share the compensation effort and set the h_{bi} to 0. In addition, as the three phase currents are unbalanced and both positive and negative sequence currents have to be considered, the instantaneous phase current peak value of each DG unit is constrained as defined in (16).

B. Tertiary Control Implementation

Based on these features, GA provides the possibility of solving a synthesized objective function with constraints included. The synthesized objective function is defined as:

$$\min f_{syn} = k_f \cdot f_{obj} + k_{GLB} \cdot g_{LB} + k_{GDG} \cdot g_{DG} + k_{GC} \cdot g_{PHC} \quad (17)$$

The constraining functions are defined as follows [28],[30]:

$$g_{LB} = \sum_{i=1}^{n} r_{LBi} \cdot \max(0, VUF_{LBi} - VUF_{LBi}^{\max}) \quad (18)$$

$$g_{DG} = \sum_{i=1}^{n} r_{DGi} \cdot \max(0, VUF_{DGi} - VUF_{DGi}^{\max}) \quad (19)$$

$$g_{PHC} = \sum_{i=1}^{n} r_{Ci} \cdot \max(0, \max\{I_{oa}, I_{ob}, I_{oc}\}_{DGi} - I_{PHi}^{\max}) \quad (20)$$

In order to evaluate the objective function and constraints, essential quantities, VUF_{LBi}, VUF_{DGi} and $\{I_{oa}, I_{ob}, I_{oc}\}_{DGi}$, need to be obtained. VUF_{LBi} and VUF_{DGi} can be calculated according to (4), (9), (10) and (14).

In order to predict the phase current $\{I_{oa}, I_{ob}, I_{oc}\}_{DGi}$, the negative sequence current of the DG unit is first calculated:

$$\dot{I}_{Si}^{N} = (\dot{V}_{Si}^{N} - \dot{V}_{LBi}^{N}) \cdot Y_{oi}^{N} \quad (21)$$

where $\dot{V}_{Si}^{N}$ and $\dot{V}_{LBi}^{N}$ can be calculated according to (9), (10) and (14), Y_{oi}^{N} can be estimated with acceptable error. The positive sequence current $\dot{I}_{Si}^{P}$ can be measured locally and sent to central controller, zero sequence current $\dot{I}_{Si}^{Z}$ can be neglected in this case. The per-phase converter current of the i^{th} DG can be calculated as:

$$\begin{bmatrix} \dot{I}_{oai} & \dot{I}_{obi} & \dot{I}_{oci} \end{bmatrix}^{T} = A \cdot \begin{bmatrix} \dot{I}_{Si}^{Z} & \dot{I}_{Si}^{P} & \dot{I}_{Si}^{N} \end{bmatrix}^{T} \quad (22)$$

Based on the description above, the simplified tertiary control scheme is generalized in Fig. 7. Essential information is first collected through LBCLs. The *Initial Calculation* block transfers the data into a desired form, obtains the total negative sequence voltage in DG sides, and perform an initial run to get an objective function value (f_{syn}^{ex}) according to the solution given by last run (TCG_{opt}^{ex}). Then GA uses the information to execute the optimization process. Mathematical model is used to help check the objective function value and get a set of solutions (*TCG*). The *Final Decision* block checks if the current run gives better solution than last run, otherwise the solution from last run is kept. This block helps to ensure that the tertiary control always provides better solutions, also in this way the frequent change of solution can be avoided. The flowchart of continuous GA is also given in Fig. 7 (b) [28].

V. Hardware-in-The-Loop Results

In order to verify the effectiveness of the method, dSPACE system based hardware-in-the-loop (HIL) simulation is conducted. The example system is shown in Fig. 3. The parameter settings are given in Tables I, II and III. The power rating and maximum phase current value of the two DG inverters are 6.5kW and 14A (peak value), respectively. The MG plant is operating with 220/380V, 50Hz. The parameters of primary, secondary and tertiary controllers are given in Table II and III. In the *Tertiary Controller* part, the constraint coefficients k_{GLB}, k_{GDG} and k_{GC} are relatively much larger than objective function coefficient k_F to prevent the violation of limits. The compensation reference VUF^{*} is set to 0.25% which keeps the lowest unbalance level in CB (CB is assumed to be *Quality A* area). The maximum allowed *VUF* on LB1 and LB2 ($VUF_{LB1}^{\max}$ and $VUF_{LB2}^{\max}$) are set to 1% and 2%, respectively, which means LB1 has a relatively higher power quality requirement than LB2 (LB1 is assumed to be *Quality B/C* area while LB2 is assumed to be standard power quality area). On DG side the *VUF* limitation ($VUF_{DG1}^{\max}$ and $VUF_{DG2}^{\max}$) and current per phase limitation ($I_{PH1}^{\max}$ and $I_{PH2}^{\max}$) are

TABLE I. POWER STAGE AND MG PLANT PARAMETERS

DG Inverter Ratings		**Inverter Output Filter**	
Power Rating (kVA)	Maximum Current per Phase (peak value/A)	*L (mH)*	*C (μF)*
6.5	14	*1.8*	*25*

MG Plant Transmission Lines						
Voltage (V)	*Frequency (Hz)*		Y_{o1} *(S)*	Y_{o2} *(S)*	Y_1 *(S)*	Y_2 *(S)*
220	*50*	*Positive Sequence*	*0 - j1.7693*	*0 - j1.7693*	*0.1282 - j0.6410*	*0.3035 - j1.7156*
		Negative Sequence	*0 + j1.7693*	*0 + j1.7693*	*0.1282 + j0.6410*	*0.3035+ j1.7156*

TABLE II. LOCAL CONTROL SYSTEM PARAMETERS

Droop Controller					*Virtual Impedance*		*Voltage Controller*			*Current Controller*		
m_D	m_P	n_P	E_0 *(V)*	ω_0*(rad/s)*	R_v *(Ω)*	L_v *(mH)*	k_{pV}	k_{rV}	ω_{cV}	k_{pI}	k_{rI}	ω_{cI}
0.00001	*0.0001*	*0.02*	$220\sqrt{2}$	2π*50*	*1*	*4*	*0.12*	*30*	*2*	*22*	*300*	*2*

TABLE III. CENTRAL CONTROL SYSTEM PARAMETERS

Secondary Controller		**Tertiary Controller**											
k_p	k_i	k_F	k_{GLB}	k_{GDG}	k_{GC}	k_{LB1} k_{LB2}	r_{LB1} r_{LB2}	r_{DG1} r_{DG2}	r_{C1} r_{C2}	$VUF_{LB1}^{\max}$	$VUF_{LB2}^{\max}$	$VUF_{DG1}^{\max}, VUF_{DG2}^{\max}$	$I_{PH1}^{\max}, I_{PH2}^{\max}$ (A)
0.5	*7*	*1*	*2*	*2*	*5*	*1*	*1*	*1*	*1*	*1%*	*2%*	*3%*	*14*
VUF(%)*		***GA** population size*			***GA** max number of iterations*				***GA** mutation rate*	***GA** fraction of population kept*			***GA** Step*
0.25		*40*			*400*				*20%*	*0.8*			*0.5 s*

respectively set to 3% and 14A (peak value) for both DGs. The coefficients k_{LB1} and k_{LB2} are set to 1 which means that if no constraint is violated the optimization control tends to control the *VUF* in LB1 and LB2 to the same level. Note that the ratio of k_{LB1} and k_{LB2} can be changed according to the relative importance of the buses.

A load change and control activation process is applied to MG plant in order to test the effectiveness of the method. The detailed load parameters and controller activation information is given in Table IV. Two types of loads are applied: type A simulates three phase balanced load, and type B is a single phase load connected between *phase A* and *phase B* in each bus. The simulation results are shown in Figs. 8-10, from *0* to *T6* different load conditions and control levels are given and activated in sequences.

TABLE IV. LOADING AND ACTIVATION PROCESS

time	LB1	LB2	CB
0	Type A: *Y=0.0050-j0.0032 S*	Type A: *Y=0.0050-j0.0032 S*	Type A: *Y=0.0005-j0.0032 S*
T1	-	-	Type B: Y_u*=0.02 S*
T2	Activate secondary unbalance compensation		
T3	Activate tertiary optimization		
T4	-	-	Type B: Y_u*=0.0143 S*
T5	-	Type A: *Y=0.0167 S*	-

A. 0~T1: balanced system

During *0~T1*, no unbalanced load is connected to the system, only balanced 3-phase loads (Type A) are connected at LB1, LB2 and CB. As can be seen in Fig. 8, the three-phase voltage and the currents are balanced. The P/Q consumption is given in Fig. 10.

B. T1~T2: unbalanced load connected to CB

During *T1~T2*, an unbalanced load (Y_u*=0.02 S*) is connected at CB which causes the increasing of *VUF* in each bus (VUF_{CB}=1.46%, VUF_{LB1}=0.39%, VUF_{LB2}=0.72%), while the *VUF* on DG sides remain unchanged. Because of the difference of transmission line parameters, *VUF* on LB1 and LB2 are different. VUF_{LB1} is smaller than VUF_{LB2}, because the transmission line between LB1 and CB has relatively smaller admittance than the one between LB2 and CB. This result is in accordance with the analysis in Fig. 5 that before compensation ($V_S^N = 0$), V_{LB1}^N is larger than V_{LB2}^N.

C. T2~T3: secondary unbalance compensation activated

During *T2~T3*, secondary compensation control is activated to compensate the unbalance on CB. *VUF* on CB is decreased to *0.25%*, while *VUF* on DG sides are increased to *1.2%*. However, VUF_{LB1} becomes larger than VUF_{LB2} after compensation (VUF_{LB1}*=0.82%*, VUF_{LB2}*=0.49%*). This process is also demonstrated in Fig. 5 that after compensation the negative sequence voltage at LB1 and LB2 may be changed in inverse direction and the absolute value of VUF_{LB1} becomes larger than VUF_{LB2}. In fact, the secondary compensation does not change current flow (as can be seen in Fig. 8 #3 and #4, the current per phase values remain unchanged before and after T2), but shifts negative sequence voltage on both DG sides equally toward negative direction in order to bring down the negative voltage level in CB. The CB voltage before and after secondary compensation are shown in Figs. 11 (a) and (b) which indicate that after compensation the voltage unbalance on CB is reduced.

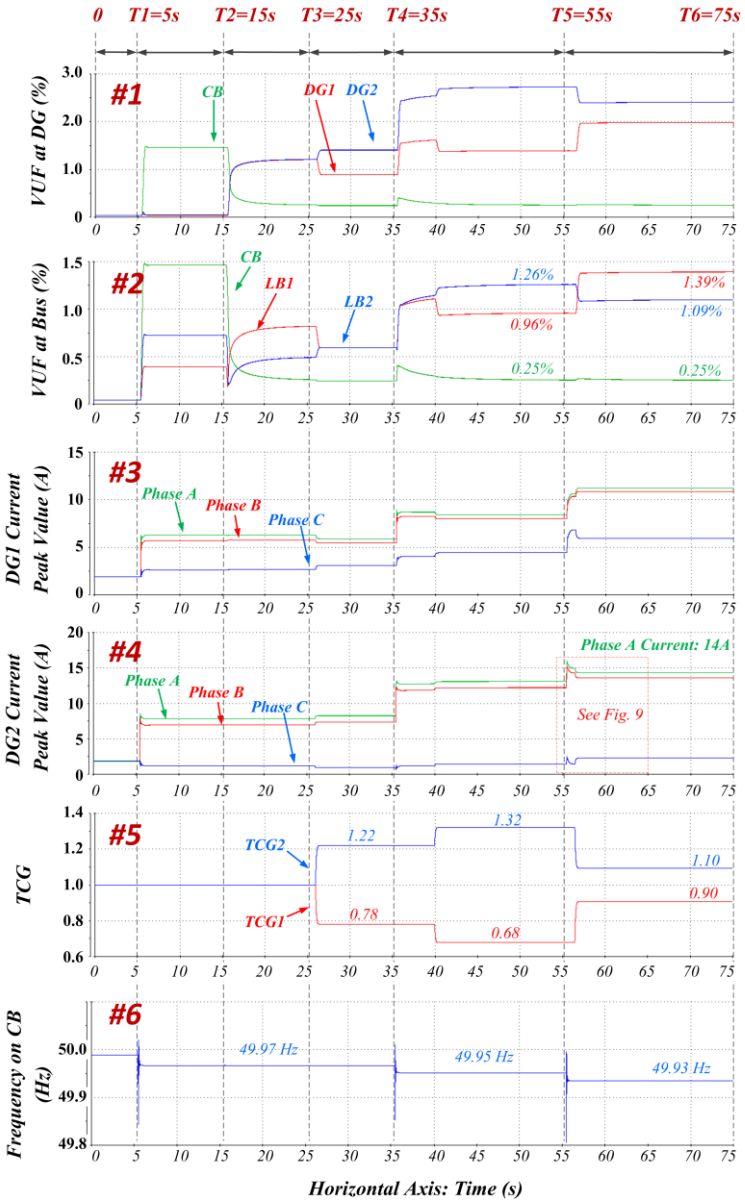

Fig. 8. Simulation Process.

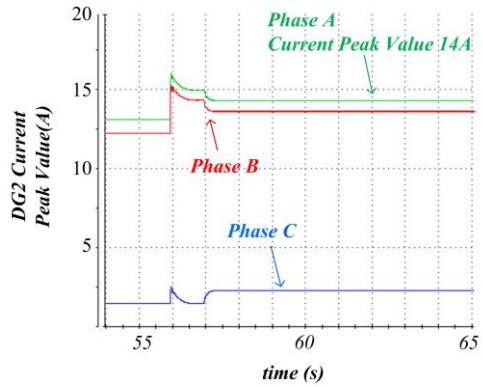

Fig. 9. Detailed phase current peak value.

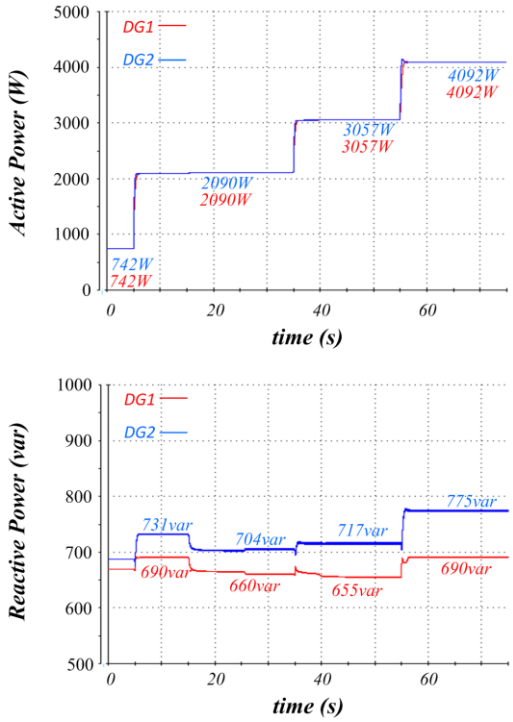

Fig. 10. Active and reactive power generation of DGs.

D. T3~T4: tertiary optimization activated

From *T3*, tertiary optimization control is activated. The objective is to control *VUF* on LB1 and LB2 to a fixed ratio (*1:1*). It can be seen in Fig. 8 that during *T3~T4*, the phase currents are all less than the limit value 14A, *VUF* at LBs and DG sides are all within limit value. Since no constraint is violated, VUF_{LB1} and VUF_{LB2} are controlled to *0.59%* equally which is in accordance with the pre-set ratio (k_{LB1}:k_{LB2}=1:1). This change is achieved by adjusting *TCG* values (*TCG1* and *TCG2* are changed to 0.78 and 1.22) to adjust the compensation efforts of DG1 and DG2. It can be seen from *#1* in Fig. 8 that the *VUF* at DG sides are changed to *0.89%* and *1.4%* whose ratio is equal to the ratio between *TCG1* and *TCG2*. The *VUF* on CB is kept at *0.25%*.

The objective function (17) is plotted in Fig. 12. In Fig. 12 (a), the objective function f_{syn} is plotted versus *TCG1* and *TCG2* to show the change of f_{syn} with *TCG* values. The white part is the near optimal region. The diagonal dashed line is the constraint of total compensation efforts (*TCG1+TCG2=2*), which means the final solution has to be located on this line. The final solution during this stage is given as $TCG1_{OPT}$=0.78, $TCG2_{OPT}$=1.22, which is located within the near optimal region. As the optimization is trying to find an optimal sharing proportion between the two DGs, in Fig. 12 (b) the objective function f_{syn} is plotted versus the ratio between *TCG1* and *TCG2* (R_{TCG}). The global optimum reaches when R_{TCG} =0.64, while the ratio between $TCG1_{OPT}$ and $TCG2_{OPT}$ is equal to 0.64. This result demonstrates that the solution given by tertiary control locates at near optimum point.

E. T4~T5: unbalanced load connected to CB

During *T4~T5*, more unbalanced load (Type B, Y_u*=0.0143 S*) is connected to CB. It can be observed in Fig. 8 that after *T4*, the *VUF* in DG terminals and LBs are increased. *VUF* in CB is fast restored to 0.25%. However, *VUF* on LB1 exceeds

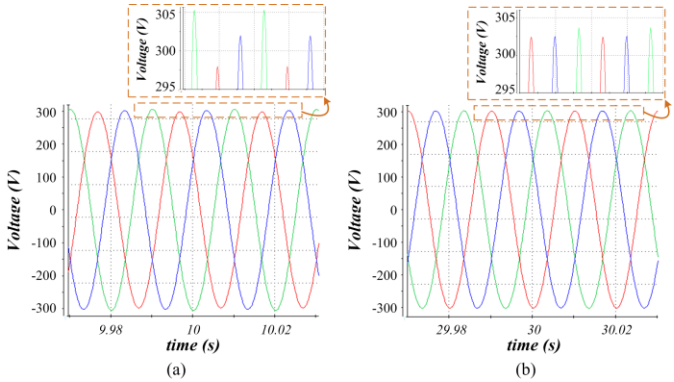

Fig. 11. CB voltage: (a) before compensation; (b) after compensation.

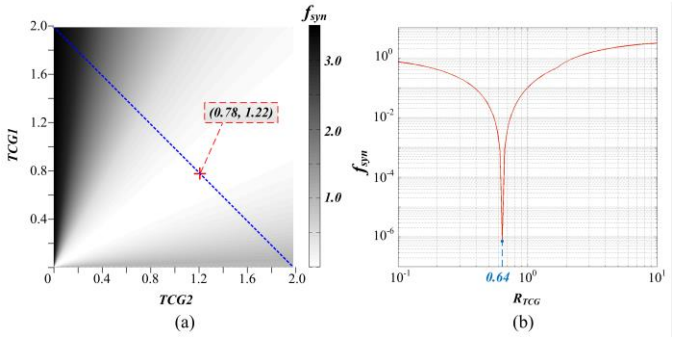

Fig. 12. Objective function during *T3~T4*: (a) f_{syn} vs. *TCG*; (b) f_{syn} vs. R_{TCG}.

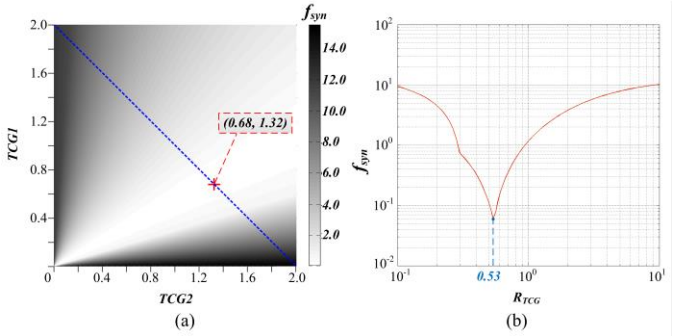

Fig. 13. Objective function during *T4~T5*: (a) f_{syn} vs. *TCG*; (b) f_{syn} vs. R_{TCG}.

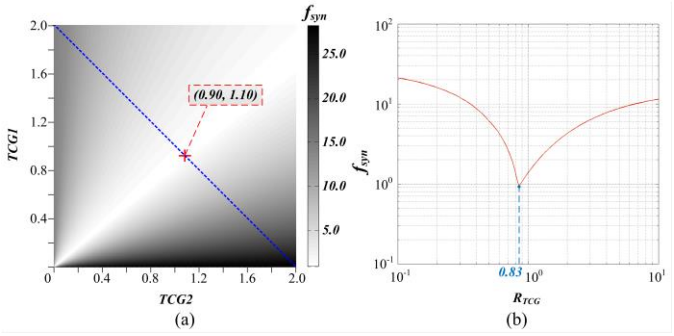

Fig. 14. Objective function during T5~T6: (a) f_{syn} vs. *TCG*; (b) f_{syn} vs. R_{TCG}.

the limitation of 1% (see *35s~40s* in *#2* in Fig. 8). *TCG*1 and *TCG*2 are changed to *0.68* and *1.32* respectively so as to restore VUF_{LB1} to 0.96%. During *40s~55s*, the system reaches steady state. The *VUF* values on LB1, LB2 and CB are 0.96%, 1.26% and 0.25% respectively.

The objective function during *T4~T5* is plotted in Fig. 13. The final solution during this stage is given as $TCG1_{OPT}$=0.68, $TCG2_{OPT}$=1.32, which is located within the near optimal region (see Fig. 13 (a)). Fig. 13 (b) shows the change of f_{syn} value with R_{TCG}. The global optimum reaches when R_{TCG} =0.53, while the ratio between $TCG1_{OPT}$ and $TCG2_{OPT}$ is equal to this value. This result demonstrates that the solution given by tertiary control locates at the near optimum point.

F. T5~T6: balanced load connected to LB2

In order to test the response of the system when the DG phase limit is violated, balanced load (Type A) is connected to LB2 at *T5*. It can be seen from *#3* in Fig. 8 and Fig. 9 that immediately after loading, *Phase A* current of DG2 exceeds the limitation of 14A, after 1s (two optimization steps) it is restored to 14A. During this process, the tertiary control changes *TCG*1 and *TCG2* to 1.10 and 0.90 to ensure the safety of DG units. However, the power quality on LB1 has to be sacrificed. After this change, the *VUF* values on LB1, LB2 and CB are changed to 1.39%, 1.09% and 0.25% respectively. When the system reaches steady state, the DG1 and DG2 current per phase values are all within 14A limit.

The objective function during *T5~T6* is plotted in Fig. 14. The final solution during this stage is given as $TCG1_{OPT}$=0.90, $TCG2_{OPT}$=1.10, which is located within the near optimal region (see Fig. 14 (a)). Fig. 14 (b) shows the change of f_{syn} value with R_{TCG}. The global optimum reaches when R_{TCG} =0.83, while the ratio between $TCG1_{OPT}$ and $TCG2_{OPT}$ is close to this value. This result demonstrates that the solution given by tertiary control locates at the near optimum point.

G. Frequency and power change

The CB frequency change is presented in #6 in Fig. 8. The nominal frequency of the MG system is 50Hz. As frequency is controlled by P^+ as shown in (1) and Fig. 2, the proposed approach has little effect over the system frequency. As can be seen from #6 in Fig. 8, the frequency change is within 0.1Hz.

The active and reactive power change during the process is shown in Fig. 10. The active power is well shared, while the reactive power sharing is affected because of the transmission line difference and the compensation effort adjustment.

H. Comparison of optimized and non-optimized system

A comparison has been made between optimized and non-optimized system from *T3* to *T5* regarding the *VUF* value in different buses, as shown in Fig. 15. The dashed curves denote the non-optimized system performance while the solid curves represent optimized system. During *T4~T5*, if tertiary optimization is not activated, the *VUF* value on LB1 exceeds the limit value of 1%, while the optimized system keeps the *VUF* on LB1 lower than the limit. At *T5*, a balanced load is connected to LB2 which causes the DG2 *Phase A* current exceeds the 14A limit in the optimized system. The optimized system has to sacrifice the power quality in LB1 so as to ensure the safety of DG2. Accordingly, the *VUF* value in LB1 exceeds the 1% limit. However, this value is still lower than the value in non-optimized system. Also during the whole process, the *VUF* in CB is kept at 0.25%. Based on the results, it is demonstrated that compared with non-optimized system, the proposed control algorithm is able to keep the *VUF* value

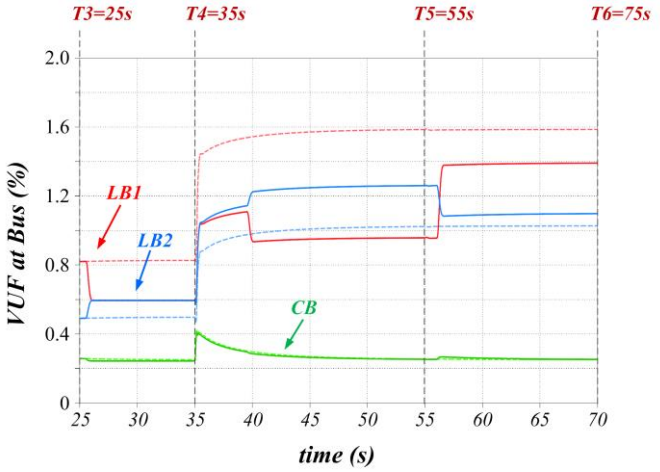

Fig. 15. Comparison between optimized and non-optimized system.

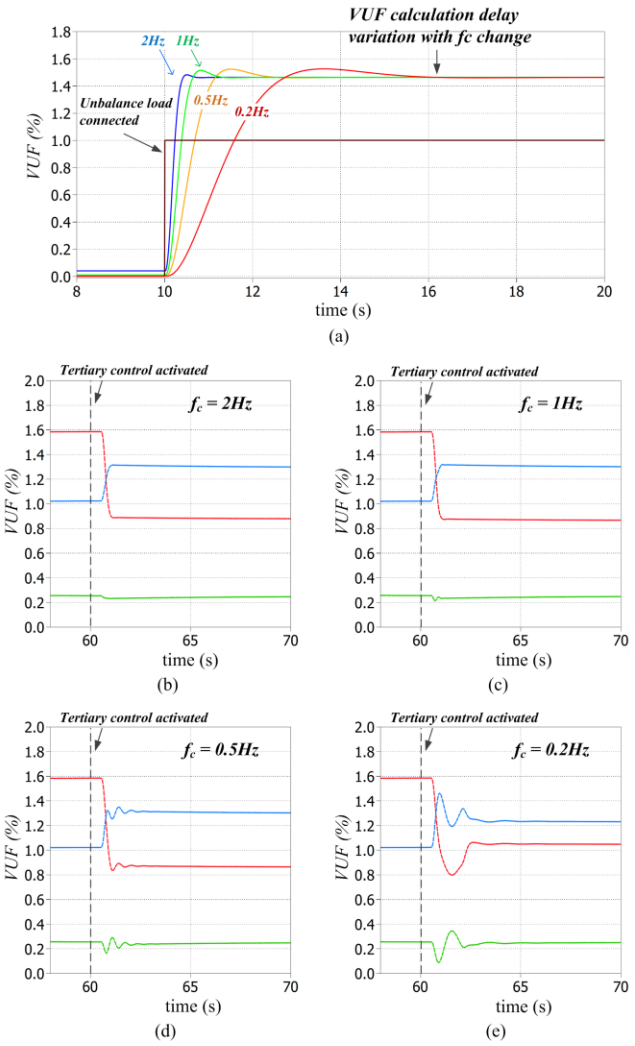

Fig. 16. System performance under different delays: (a) VUF calculation delay under different f_c; (b) Tertiary control under f_c=2Hz; (c) Tertiary control under f_c=1Hz; (d) Tertiary control under f_c=0.5Hz; (e) Tertiary control under f_c=0.2Hz.

within limit when the DGs are capable of providing compensation support.

I. System performance under different delays

As the secondary and tertiary controllers are based on the knowledge of the system, the calculation delay has certain influence over the system performance. The delay of the calculation is mainly caused by the LPFs used in the *dq components extraction* block as shown in Fig. 2. The cut-off frequency of the LPFs is set to f_c = 2Hz in this paper. In Fig. 16 (a) the cut off frequency (f_c) of the LPFs is changed from 0.2~2Hz to emulate different calculation delays and communication delays. With the decreasing of f_c, the *VUF* delay becomes larger. In this paper, the tertiary optimization algorithm runs every 0.5s, which is much slower compared with secondary controller. The performances of tertiary control under different f_c values are shown in Figs. 16 (b)-(e). Within the range f_c = 0.2-2Hz, the tertiary control is able to perform effectively.

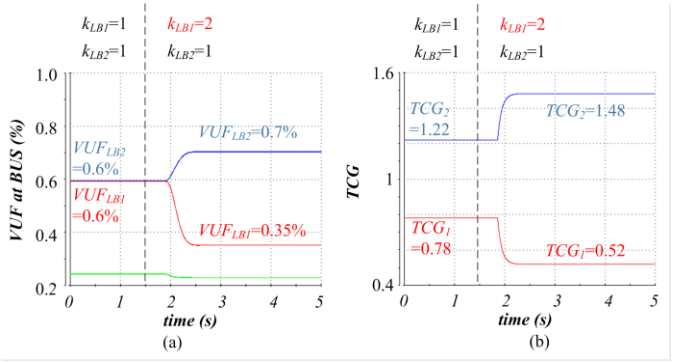

Fig. 17. System performance with different bus importance ratio k_{LBi}: (a) VUF on LB change under different k_{LBi}; (b) optimal TCG solution change under different k_{LBi}.

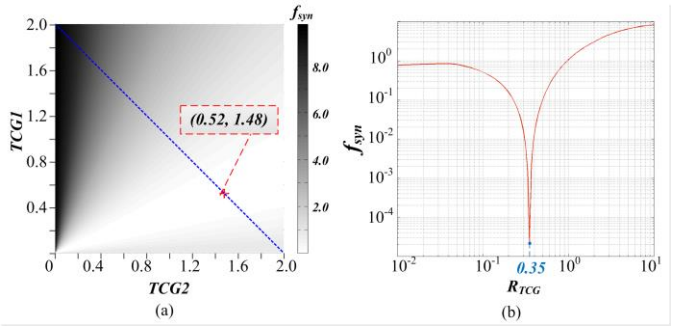

Fig. 18. f_{syn} plot after k_{LBi} change: (a) f_{syn} vs. *TCG*; (b) f_{syn} vs. R_{TCG}.

J. System performance under different k_{LBi}

In order to verify the system response with different k_{LBi}, HIL results are shown in Fig. 17. The system starts with the same bus importance ratio (k_{LB1}= k_{LB2}=1), the *VUF* values in LB1 and LB2 are controlled to the same level (0.6%). After the change of k_{LB1} (k_{LB1} is changed from 1 to 2, which means LB1 has relative higher importance than LB2, VUF_{LB1} should be kept lower than VUF_{LB2}), the optimization algorithm finds a new solution ($TCG1_{OPT}$=0.52, $TCG2_{OPT}$ =1.48) during next run, changing the *VUF* values to VUF_{LB1}=0.35%, VUF_{LB2} =0.70%. The objective function is plotted in Fig. 18, which demonstrates that the solution given by GA is located at near global optimum region.

VI. Conclusion

This paper proposes a hierarchical control to realize

optimal voltage unbalance compensation in islanded microgrids. The proposed hierarchy includes three levels: primary level for negative sequence power sharing control, secondary level for unbalance compensation control and tertiary level for global power quality optimization.

The general idea of this method is to assign a *TCG* for each DG, and common compensation reference given by secondary control is first multiplied by *TCG* and then sent to respective DG. The tertiary control inherently is an optimization solver. Accordingly, it is necessary to build a mathematical model to establish a link between *TCG* and *VUF* on DG sides and buses. An example system is modeled and simulated with all the control levels. HIL results are presented to demonstrate that the proposed method is capable of controlling the unbalance level on each bus according to their limitations and power quality requirements.

This method realizes accurate unbalance control among buses in an islanded system considering different power quality requirements of the buses and compensation limitation of DGs. This method also enables the possibility of higher level scheduling and management for power quality control in microgrids to realize economic and technical objectives.

VII. Appendix

The detailed matrices used in (3) are described as follows:

$$Y_{ph}=\begin{bmatrix} Y+Y_u & -Y_u & 0 \\ -Y_u & Y+Y_u & 0 \\ 0 & 0 & Y \end{bmatrix},\ V_{ph}=\begin{bmatrix} V_a-V_{nn} \\ V_b-V_{nn} \\ V_c-V_{nn} \end{bmatrix},$$

$$A=\begin{bmatrix} 1 & 1 & 1 \\ 1 & a^2 & a \\ 1 & a & a^2 \end{bmatrix}$$

The detailed parameters used in (8) are described as follows:

$$K_1=\frac{Y_1^N}{Y_1^N+Y_{o1}^N},\ K_2=\frac{Y_2^N}{Y_2^N+Y_{o2}^N},\ K_3=K_1\cdot Y_{o1}^N,\ K_4=K_2\cdot Y_{o2}^N$$

VIII. References

[1] *IEEE Guide for Design, Operation, and Integration of Distributed Resource Island Systems with Electric Power Systems*, IEEE Standard 1547.4-2011, July 2011.

[2] R. H. Lasseter, "Smart Distribution: Coupled Microgrids," *Proceedings of the IEEE*, vol.99, pp. 1074-1082, June 2011.

[3] F. Barrero, S. Martinez, F. Yeves, F. Mur, P. M. Martinez, "Universal and reconfigurable to UPS active power filter for line conditioning," *IEEE Trans. Power Deliv.*, vol. 18, pp. 283–290, 2003.

[4] D. Graovac, V. Katic, A. Rufer, "Power Quality Problems Compensation With Universal Power Quality Conditioning System," *IEEE Trans. Power Deliv.*, vol. 22, pp. 968-976, April 2007.

[5] B. Singh, K. Al-Haddad, A. Chandra, "A review of active filters for power quality improvement," *IEEE Trans. Ind. Electron.*, vol.46, no.5, pp. 960-971, Oct 1999.

[6] A. Garcia-Cerrada, O. Pinzon-Ardila, V. Feliu-Batlle, P. Roncero-Sanchez, P. Garcia-Gonzalez, "Application of a Repetitive Controller for a Three-Phase Active Power Filter," *IEEE Trans. Power Electron.*, vol.22, pp. 237-246, Jan. 2007.

[7] B. Singh, J. Solanki, "An Implementation of an Adaptive Control Algorithm for a Three-Phase Shunt Active Filter," *IEEE Trans. Ind. Electron.*, vol.56, pp. 2811-2820, Aug. 2009.

[8] S. George, V. Agarwal, "A DSP Based Optimal Algorithm for Shunt Active Filter Under Nonsinusoidal Supply and Unbalanced Load Conditions," *IEEE Trans. Power Electron.*, vol.22, pp. 593-601, March 2007.

[9] J. He, Y. Li, M. S. Munir, "A Flexible Harmonic Control Approach Through Voltage-Controlled DG–Grid Interfacing Converters," *IEEE Trans. Ind. Electron.*, vol.59, pp. 444-455, Jan. 2012.

[10] P. Cheng, C. Chen, T. Lee, S. Kuo, "A Cooperative Imbalance Compensation Method for Distributed-Generation Interface Converters," *IEEE Trans. Ind. Appl.*, vol.45, pp. 805-815, March-april 2009.

[11] J. M. Guerrero, P. C. Loh; T. Lee; M. Chandorkar, "Advanced Control Architectures for Intelligent Microgrids—Part II: Power Quality, Energy Storage, and AC/DC Microgrids," *IEEE Trans. Ind. Electron.*, vol.60, pp. 1263-1270, April 2013.

[12] M. Prodanovic, T. C. Green, "High-Quality Power Generation Through Distributed Control of a Power Park Microgrid," *IEEE Trans. Ind. Electron.*, vol.53, pp. 1471-1482, Oct. 2006.

[13] R. Majumder, A. Ghosh, G. Ledwich, F. Zare, "Load sharing and power quality enhanced operation of a distributed microgrid," *IET Renew. Power Gener.*, vol.3, pp. 109-119, June 2009.

[14] M. Hamzeh, H. Karimi, H. Mokhtari, "A New Control Strategy for a Multi-Bus MV Microgrid Under Unbalanced Conditions," *IEEE Trans. Power Syst.*, vol.27, pp. 2225-2232, Nov. 2012.

[15] M. Savaghebi, A. Jalilian, J. C. Vasquez, J. M. Guerrero, "Secondary Control Scheme for Voltage Unbalance Compensation in an Islanded Droop-Controlled Microgrid," *IEEE Trans. Smart Grid*, vol.3, pp. 797-807, June 2012.

[16] M. Savaghebi, A. Jalilian, J. C. Vasquez, J. M. Guerrero, "Autonomous Voltage Unbalance Compensation in an Islanded Droop-Controlled Microgrid," *IEEE Trans. Ind. Electron.*, vol.60, pp. 1390-1402, April 2013.

[17] *Electric Power Systems and Equipment—Voltage Ratings (60 Hertz)*, ANSI Standard Publication no. ANSI C84.1-1995.

[18] C. Marnay, "Microgrids and Heterogeneous Security, Quality, Reliability, and Availability," *in 2007 Power Conversion Conference - Nagoya*, pp. 629-634.

[19] Y. Hayashi, T. Ise, K. Tsuji, K. Shimizu, F. Inui, "A power control scheme between quality control centers in FRIENDS," *Elect. Eng. Jpn.*, vol. 151, pp. 20-31, 2005.

[20] K. Hirose, A. Fukui, A. Matsumoto, H. Murai, T. Takeda, T. Matsumura, "Development of Multiple Power Quality Supply System," *IEEJ Trans. Electr. Electron. Eng*, vol. 5, pp. 523-530, 2010.

[21] K. Hirose, T. Takeda, A. Fukui, "Field demonstration on multiple power quality supply system in Sendai, Japan," *in 2007 9th International Conference on Electrical Power Quality and Utilisation, EPQU*, 2007.

[22] S. Papathanassiou, N. Hatziargyriou, K. Strunz, "A Benchmark Low Voltage Microgrid Network", *CIGRE Symposium*, Athens, 13-16 April 2005.

[23] A. Bidram, A. Davoudi, "Hierarchical Structure of Microgrids Control System," *IEEE Trans. Smart Grid*, vol.3, pp. 1963-1976, Dec. 2012.

[24] H. Akagi, Y. Kanazawa, A. Nabae, "Instantaneous Reactive Power Compensators Comprising Switching Devices without Energy Storage Components," *IEEE Trans. Ind. Appl.*, vol.IA-20, pp. 625-630, May 1984.

[25] A. von Jouanne, B. Banerjee, "Assessment of voltage unbalance," *IEEE Trans. Power Delivery*, vol.16, pp. 782-790, Oct 2001.

[26] J. D. Glover, M. S. Sarma, T. J. Overbye. *Power System Analysis and Design*, vol. 4, 2008, p. 400.

[27] *IEEE Standard for Interconnecting Distributed Resources with Electric Power Systems*, IEEE Std 1547-2003, pp. 1-28, July 2003.

[28] R. L. Haupt, S. E. Haupt, *Practical Genetic Algorithms*. (2nd ed.) [Online]. Available: http://onlinelibrary.wiley.com/book/10.1002/0471671746;jsessionid=68B5F5913141E057EEE8CC9161628F2F.f01t03. [Accessed: 21-Apr-2014].

[29] Z. Michalewicz, M. Schoenauer, "Evolutionary algorithms for constrained parameter optimization problems", *Evolutionary Computation*, vol. 4, pp. 1-32, 1996.

[30] C. A. Coello Coello, "Theoretical and numerical constraint-handling techniques used with evolutionary algorithms: a survey of the state of the art," *Comput. Methods Appl. Mech. Eng.*, vol. 191, pp. 1245-1287, 2002.

[31] N. R. Ullah, K. Bhattacharya, T. Thiringer, "Wind Farms as Reactive Power Ancillary Service Providers—Technical and Economic Issues," *IEEE Trans. Energy Convers.*, vol.24, pp. 661-672, Sept. 2009

[32] V. Calderaro, V. Galdi, G. Massa, A. Piccolo, "Distributed generation and local voltage regulation: An approach based on sensitivity analysis," *2011 2nd IEEE PES Int. Conf. Exhib. Innov. Smart Grid Technol.*, pp. 1–8, 2011.

[33] V. Calderaro, V. Galdi, G. Massa, and A. Piccolo, "Distributed generation management: An optimal sensitivity approach for decentralized power control," *in IEEE PES Innovative Smart Grid Technologies Conference Europe*, 2012.

[34] V. Calderaro, G. Conio, V. Galdi, G. Massa, and A. Piccolo, "Optimal Decentralized Voltage Control for Distribution Systems With Inverter-Based Distributed Generators," *IEEE Trans. Power Syst.*, vol. 29, pp. 230-241, 2014.

IX. BIOGRAPHIES

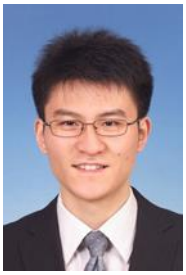

Lexuan Meng received the B.S. degree in Electrical Engineering and M.S. degree in Electrical Machine and Apparatus from Nanjing University of Aeronautics and Astronautics (NUAA), Nanjing, China, in 2009 and 2012, respectively. He is currently working toward his Ph.D. at the Department of Energy Technology, Aalborg University, Denmark. He is member of the Denmark Microgrids Research Programme in Aalborg University (www.microgrids.et.aau.dk).

His research is focusing on the tertiary control for microgrids, including power quality regulation and optimization, as well as the applications of distributed control and communication algorithms.

Fen Tang received the B.S. degree in Electrical Engineering and the Ph.D. degree in Power Electronics & Electric Drives from Beijing Jiaotong University, Beijing, China, in 2006 and 2013, respectively. She is currently a Postdoc in Beijing Jiaotong University. From Jan. 2013 to Jan. 2014 she was a guest Postdoc at Department of Energy Technology, Aalborg University, Denmark.

Her research interests include microgrid, wind power generation system, power converter for renewable generation systems, power quality, and motor control.

Mehdi Savaghebi was born in Karaj, Iran, in 1983. He received the B.Sc. degree from University of Tehran, Iran, in 2004 and the M.Sc. and Ph.D. degrees with highest honors from Iran University of Science and Technology, Tehran, Iran in 2006 and 2012, respectively, all in Electrical Engineering. From 2007 to 2014, he was a Lecturer in Electrical Engineering Department, Karaj Branch, Islamic Azad University where he taught various courses and conducted research on power systems and electrical machines. In 2010, he was a Visiting Ph.D. Student with the Department of Energy Technology, Aalborg University, Aalborg, Denmark and with the Department of Automatic Control Systems and Computer Engineering, Technical University of Catalonia, Barcelona, Spain.

Currently, he is a Postdoctoral Research Assistant in Department of Energy Technology, Aalborg University. His main research interests include distributed generation systems, microgrids and power quality issues of electrical systems.

Juan C. Vasquez (M'12) received the B.S. degree in Electronics Engineering from Autonomous University of Manizales, Colombia in 2004 where he has been teaching courses on digital circuits, servo systems and flexible manufacturing systems. In 2009, He received his Ph.D degree from the Technical University of Catalonia, Barcelona, Spain in 2009 at the Department of Automatic Control Systems and Computer Engineering, from Technical University of Catalonia, Barcelona (Spain), where he worked as Post-doc Assistant and also teaching courses based on renewable energy systems. Since 2011, he has been an Assistant Professor in microgrids at the Institute of Energy Technology, Aalborg University, Aalborg, Denmark, where he is the co-responsible of the microgrids research program. His current research interests include operation, power management, hierarchical control and optimization applied to Distributed Generation in AC/DC microgrids. He is currently member of the Technical Committee on Renewable Energy Systems TC-RES.

Josep M. Guerrero (S'01-M'04-SM'08) received the B.S. degree in telecommunications engineering, the M.S. degree in electronics engineering, and the Ph.D. degree in power electronics from the Technical University of Catalonia, Barcelona, in 1997, 2000 and 2003, respectively. Since 2011, he has been a Full Professor with the Department of Energy Technology, Aalborg University, Denmark, where he is responsible for the Microgrid Research Program. From 2012 he is a guest Professor at the Chinese Academy of Science and the Nanjing University of Aeronautics and Astronautics; and from 2014 he is chair Professor in Shandong University.

His research interests is oriented to different microgrid aspects, including power electronics, distributed energy-storage systems, hierarchical and cooperative control, energy management systems, and optimization of microgrids and islanded minigrids. Prof. Guerrero is an Associate Editor for the IEEE TRANSACTIONS ON POWER ELECTRONICS, the IEEE TRANSACTIONS ON INDUSTRIAL ELECTRONICS, and the IEEE Industrial Electronics Magazine, and an Editor for the IEEE TRANSACTIONS on SMART GRID. He has been Guest Editor of the IEEE TRANSACTIONS ON POWER ELECTRONICS Special Issues: Power Electronics for Wind Energy Conversion and Power Electronics for Microgrids; the IEEE TRANSACTIONS ON INDUSTRIAL ELECTRONICS Special Sections: Uninterruptible Power Supplies systems, Renewable Energy Systems, Distributed Generation and Microgrids, and Industrial Applications and Implementation Issues of the Kalman Filter; and the IEEE TRANSACTIONS on SMART GRID Special Issue on Smart DC Distribution Systems. He was the chair of the Renewable Energy Systems Technical Committee of the IEEE Industrial Electronics Society. In 2014 he was awarded by Thomson Reuters as ISI Highly Cited Researcher.